Stereoisomer-dependent rate coefficients and reaction mechanisms of 2-ethyloxetanylperoxy radicals

Anna C. Donera, Judit Zádorb, and Brandon Rotaveraa, c, *

^aUniversity of Georgia, Department of Chemistry, Athens, Georgia, USA ^bSandia National Laboratories, Combustion Research Facility, Livermore, California, USA ^cUniversity of Georgia, College of Engineering, Athens, Georgia, USA

Abstract

Cyclic ethers undergo H-abstraction reactions that yield carbon-centered radicals (\dot{R}). The ether functional group introduces a competing set of reaction pathways: ring-opening and reaction with O₂ to form peroxy radical adducts, ROÖ, which can result in stereoisomers. ROÖ derived from cyclic ethers can subsequently isomerize into hydroperoxy-substituted carbon-centered radicals, QOOH, which can also undergo ring-opening reactions or pathways prototypical to alkyl oxidation. The balance of reactions that unfold from cyclic ether radicals depends intrinsically on the size of the ring and the structure of any substituents retained in the formation step. The present work examines unimolecular reactions of peroxy radicals from 2-ethyloxetane, a four-membered cyclic ether formed during n-pentane oxidation, and reveals stereoisomer-specific reaction pathways.

Automated quantum chemical computations were conducted on constitutional and stereoisomers of ROÖ derived from O₂-addition to 2-ethyloxetanyl radicals. Pressure-dependent rate calculations were conducted by solving the master equation from 300 – 1000 K and from 0.01 – 100 atm. Branching fractions were then calculated at 650 K and 825 K, the peak temperatures at which cyclic ethers form in alkane oxidation. Isomer-specific reaction pathways of *anti*-ROO and *syn*-ROO and resulting impact on radical production were evident. QOOH ring-opening reactions were significant as were rates of bi-cyclic ether formation common in alkyl radical oxidation.

Detailed prescription of rates and reaction mechanisms describing cyclic ether consumption mechanisms are important to enable accurate modeling of reactions of ephemeral QOOH radicals because of the direct, isomerspecific formation pathways. In addition, detailed cyclic ether mechanisms are required to reduce mechanism truncation error. The results herein provide insight on connections between cyclic ethers and chain-reaction pathways yielding OH, HOO, and other radicals, in addition to pathways leading to performic acid (HOOC(=O)H), the decomposition of which via O–O scission results in an exothermic, chain-branching step.

<i>Keywords:</i> QOOH; mechanism truncation error; <i>n</i> -pentane; Kinbot; chemical kinetics modeling								

^{*}Corresponding author.

Information for Colloquium Chairs and Cochairs, Editors, and Reviewers

1) Novelty and Significance Statement

Novelty:

- We provide the first set of electronic structure calculations on R and ROO radicals derived from oxidation of 2-ethyloxetane, which aids in the improvement of chemical kinetics models.
- This work provides new insight on stereoisomer-dependent chemical kinetics of cyclic ethers.
- We uncover new, direct pathways from cyclic ethers to small ketohydroperoxides that may contribute to chain-branching.

Significance: Because they are direct products of QOOH decomposition, alkyl-substituted cyclic ethers are critical modeling targets for low-temperature combustion experiments. We show in this work that O₂-addition to cyclic ether radicals is competitive with unimolecular decomposition below 1000 K. Furthermore, alkyl-substituted cyclic ether peroxy radical chemistry is highly sensitive to the starting diastereomer.

In the present work, we examine the mechanisms and kinetics of 2-ethyloxetanylperoxy radicals. Unlike 2,4-dimethyloxetane, 2-ethyloxetane has only one chiral center, i.e. no diastereomers. However, the present work clearly demonstrates dramatic stereochemical effects, originating in the O₂-addition step. The ethyl substituent permits a third class of reactions of alkyl-substituted oxetanylperoxy radicals, beyond conventional QOOH decomposition products and ring-opening products, yielding small oxetane-containing species. Finally, we identify a highly favorable pathway to the small ketohydroperoxide performic acid, whose impact on ignition is unaccounted for and of potentially significant impact as a source chain-branching.

2) Author Contributions

- AD: Writing/Draft, Methodology, Modeling, Formal Analysis
- JZ: Methodology, Formal Analysis, Writing/Editing
- BR: Conceptualization, Methodology, Formal Analysis, Writing/Editing

3) Authors' Preference and Justification for Mode of Presentation at the Symposium

The authors prefer the oral presentation paper (OPP) option at the Symposium, for the following reasons:

- We highlight clear, fundamental kinetics questions that will spur research activities of experimentalists and theoreticians.
- 2. Presentation of the findings in this theoretical work will motivate the community for experimental studies on 2-ethyloxetane.
- 3. Our paper produces new insight that stimulates efforts on the expansion of sub-mechanisms for cyclic ethers in detailed chemical kinetics mechanisms of hydrocarbons and biofuels.
- 4. We contribute to three of the four themes of the 40th Symposium: *Combustion Fundamentals*, *Combustion Research Tools*, and *Combustion Impact and Mitigation*. Our paper is not part of a broader set of work requiring extensive background for an engaging presentation.

1. Introduction

Cyclic ethers are prevalent next-generation biofuels and are also intermediates formed in a chain-propagating step coincident with OH [1] during low-temperature combustion, which is initiated by the formation of peroxy radicals (ROO) and subsequent isomerization into carbon-centered radicals (QOOH). Depending on the position of the –OOH group relative to the radical center in QOOH, the structure of the substituent(s) appended to a cyclic ether varies. As a result, the degree to which prototypical alkyl oxidation reactions compete with cyclic ether ring-opening reactions depends inherently on substituent structure, with length playing a significant role.

The relevance of cyclic ether functional group effects extends beyond implications on biofuel combustion modeling [2]. In the context of hydrocarbon oxidation, while formation pathways of cyclic ethers from QOOH are routinely included in chemical kinetics mechanisms, subsequent detailing of consumption mechanisms are inadequate [3-5]. Expanding the sub-mechanisms of cyclic ethers contained within hydrocarbon reaction mechanisms directly impacts predictions of critical metrics such as ignition delay times and species profiles [5]. The effect is attributable to the inclusion of H-abstraction reactions yielding isomer-specific cyclic ether radical reaction pathways involving O2. Increasing the level of detail to describe cyclic ether reactions affords the ability to constrain theoretical rates for unimolecular reactions of QOOH [5]. In addition, an increase in the complexity of cyclic ether sub-mechanisms also impacts the predictions of species related to chainbranching pathways, including the formation of intermediates (dicarbonyls) that are ascribed to ketohydroperoxide decomposition [6, 7]. As a result, understanding elementary reactions of cyclic ether radicals is necessary to increase the fidelity of combustion modeling below 1000 K.

Fundamental insight on reaction mechanisms of alkyl-substituted oxetanes at combustion-relevant conditions remains scant. Doner et al. [8] conducted time-resolved speciation measurements on Cloxidation of 2-methyloxetane, intermediate from n-butane oxidation, and also conducted stationary point calculations at the CCSD(T)-F12/ccpVDZ-F12 level of theory to map potential energy surfaces of the corresponding R and ROO radicals. Electronic energies for stationary points along pathways to species from ring-opening reactions of R and QOOH were computed, some of which were detected in the experiments. From the latter reaction type, energetically favorable pathways to ketohydroperoxide species (performic acid and 2hydroperoxyacetaldehyde) were revealed, which may provide additional chain-branching. In addition, direct and low-lying pathways from QOOH to dicarbonyl species (3-oxobutanal and 2-methylpropanedial), which often serve as proxies for modeling reaction rates of ketohydroperoxides, were also computed. Reactions of an analogous species,

dimethyloxetane, formed from *n*-pentane oxidation, were also examined by Doner et al. [6, 7] using quantum chemical computations to produce potential energy surfaces from which pressure-dependent rate coefficients were derived.

Stereochemistry is an integral part of cyclic ether peroxy radical reactions owing to *syn*- and *anti*-isomers that can form upon O₂-addition [7, 9] and is an important aspect in determining the extent to which OH is produced. The subsequent availability of certain reaction pathways often depends on the initial isomeric structure of the peroxy adduct, *syn*-ROO or *anti*-ROO, due to the accessibility of an H-atom in the isomerization step required to form QOOH.

To examine the effect of substituent length on alkyl-substituted oxetane reactions at combustion conditions for the first time, the present work conducts quantum chemical computations on peroxy radicals produced from 2-ethyloxetane, a cyclic ether formed during *n*-pentane oxidation. Resulting from concerted ring-closure and OH loss, such as from the QOOH, 1-hydroperoxy-pent-3-yl, 2-ethyloxetane is formed in a chain-propagating step (Fig. 1). The present work computes stationary point energies along potential energy surfaces for all peroxy radical isomers of 2-ethyloxetane in order to calculate rate coefficients utilized to produce branching fractions from which inference is drawn on competing reaction pathways and radical generation.

Figure 1. Formation pathway to 2-ethyloxetane from a $\dot{Q}OOH$ isomer derived reaction of O_2 with 1-pentyl. Numerical designations indicate distinct abstraction sites.

2. Theoretical approach

The sections below detail the construction of the potential energy surfaces with KinBot [10, 11], (Section 2.1), master equation rate calculations (Section 2.2), and branching fraction calculations (Section 2.3) similar to the approach of Doner et al. [4, 9].

2.1 potential energy surfaces

The reactive potential energy surfaces for each of the seven 2-ethyloxetanylperoxy radicals formed via H-abstraction from 2-ethyloxetane followed by O₂-addition were explored automatically with the open-source code, KinBot [10, 11]. All DFT calculations were performed with Gaussian 16 [12], while all coupled cluster calculations were performed with ORCA [13].

The starting radical structure was optimized at L1 = B3LYP/6-31+G. Then a conformer search was conducted at L1. The lowest energy conformer structure was then re-optimized at L2 = ω B97X-D/6-311++G(d,p). The electronic energy, frequencies,

zero-point energy correction (0 K), and hindered rotor scans were computed at L2. The final electronic energy was computed at L3 = CCSD(T)-F12a/cc-pVDZ-F12. The energy values, E, are represented by **Eqn. 1**, where E_c is the electronic energy, and ZPE is the zero-point energy correction.

$$E = E_e(L3//L2) + ZPE(L2//L2)$$
 (1)

Uncertainty typical for the level of theory herein is ~1 kcal/mol for species with, at most, moderate multireference character. The conformational search was performed on a 60° (6 points) grid. Ring conformers were generated by systematically distorting the backbone of the ring. When determining the number of ring conformers to generate, the following rules were used. For 3-membered rings, no ring conformers were generated. For 4-, 5-, and 6membered rings the number of trial ring conformers was calculated as $3^{n_{\text{ring}}-3}$, where n_{ring} is the size of the ring. For fused rings, the size of the smallest complete ring was taken. Conformer sampling was conducted in order to select the lowest energy structure. The conformers of the acyclic substituents of each ring conformer are then sampled on the 60° grid. However, for cases where the predicted number of conformers exceeded 300, then 300 points on the grid were randomly selected.

For each rotor, the energy was calculated for 24 dihedral angles separated by 15°. All degrees of freedom except the scanned dihedral were relaxed. Failed points were approximated using interpolation based on a Fourier fit. The motion along the rotors at the minimum was projected out from the Hessian to arrive at the reduced set of harmonic frequencies. In the case that KinBot determines a lower energy conformer during hindered rotor scans at 0 K, the new, lower energy conformer replaced the prior one.

Reaction classes from templates were used to construct initial saddle point guesses for a given well. The initial saddle point guess is constructed by a series of constrained optimization steps at the L0 = AM1 level of theory. The initial guess is refined to a true first-order-saddle-point (FOSP) at the L1 = B3LYP/6-31+G level of theory and confirmed by intrinsic reaction coordinate (IRC) calculations at the same level. The stereochemistry of the reactant from the IRC calculation is compared with the stereochemistry of the current initial well geometry. For cases with more than one chiral center, transition states that lead to switched stereochemistry are discarded. Inversion between diastereomers was not considered because the tertiary oxetane radicals are approximately planar, and inversion not about a tertiary radical incurs a large barrier.

Two conditions were required for a product well to be included and followed on the potential energy surfaces. The first is that the L1 barrier height leading to the product well is less than an energy threshold, set to the $\dot{R}+O_2\to RO\dot{O}$ well depth computed at the L3 level of theory. The second condition for inclusion

of a product well was that the predicted branching fraction from the reactant well was >5% at the high-pressure limit at 400 K or 1000 K. The branching fractions required for this condition were computed by solving the master equation constructed with the L2 level stationary points directly connected to the current reactant well. While any trimming algorithm inherently carries some risk of ignoring potentially important side reactions, considering the computational cost and the intended application, approach herein is likely to yield an adequate and rigorously built sub-mechanism for the target species.

Throughout the present work, 2-ethyloxetanyl radicals are named RX where X is the carbon number (Fig. 1) from which H is abstracted from 2-ethyloxetane. 2-ethyloxetanylperoxy radicals are labeled ROOX where X is the carbon number to which O₂ adds to 2-ethyloxetanyl radicals. The hydroperoxyalkyl radicals that form from 2-ethyloxetanylperoxy radicals are labeled QOOHXY where X is the carbon number where the hydroperoxyl group is position and Y is the carbon number where the radical site is located.

2.2 master equation rate calculations

The master equations were solved with the MESS software [14] from 300 K to 1000 K in 50-K increments and spanning five orders of magnitude in pressure, from 0.01 atm to 100 atm. Several parameters were estimated by empirical procedures from the literature, as discussed below. Asymmetric Eckart tunneling corrections were applied for each transition state.

Phase Space Theory [15] was used to estimate the rate coefficients for O₂-addition by scaling to analogous experimental rate coefficients. **Table 1** gives the rate analogous rate coefficients and reference for each R + O₂ reaction in the present work.

Table 1. Analogous experimental rate coefficients used to estimate O_2 addition rates with Phase Space Theory.

R	ROO	Assigned Rate	Reference
		Coefficient, k (cm ³ s ⁻¹)	
R1	anti-ROO1	7.5×10 ⁻¹²	cyclopentyl + O ₂
	syn-ROO1		[16]
R2	anti-ROO2	7.5×10 ⁻¹²	cyclopentyl + O ₂
	syn-ROO2		[16]
R3	ROO3	2.0×10 ⁻¹¹	tert-butyl + O ₂ [17]
R4	ROO4	1.7×10 ⁻¹¹	2-butyl + O ₂ [17]
R5	ROO5	7.5×10 ⁻¹²	1-butyl + O ₂ [17]

Collision parameters were selected according to the procedure described by Jasper [18] for hydroperoxides. The average downward energy transfer α was calculated between 300 K and 1000 K and fit to the form $\alpha_0 (T/300 \, K)^n$. The energy relaxation factor α_0 and power n depend on the equilibrium distance σ , the well depth ε and the effective number of heavy atoms $N_{\rm eff}$.

Table 2. Collision parameters.

Species	σ (Å)	ε (K)	$N_{ m eff}$	α_0	n	α-fit
				(cm ⁻¹)		RMS
						(cm ⁻¹)
anti-ROO1	4.62	248	3 2/3	260	0.54	5.4
syn-ROO1						
anti-ROO2						
syn-ROO2						
ROO3	4.62	248	3 1/6	239	0.59	5.0
ROO4						
ROO5	4.62	248	4 1/6	280	0.52	5.7

2.3 branching fractions

Branching fractions were calculated by solving the differential equations of the master equation solution at two temperatures, 650 K and 825 K, 20 ms, $O_2 = 10^{12}$ molecules cm⁻³, and atmospheric pressure.

3. Results

The results are presented in three sections: potential energy surfaces (Section 3.1), theoretical rate coefficients (Section 3.2), and branching fractions (Section 3.3). In Section 3.1, the main reaction classes are summarized. Detailed potential energy surfaces are in S1. In Section 3.2, the largest several rate coefficients for each peroxy radical are given. In Section 3.3, the branching fractions are summarized by product type.

3.1 potential energy surfaces

Each of the entrance channels are between 33-34 kcal/mol above the respective peroxy radical well-depths except for the tertiary radical, $R3+O_2 \rightarrow ROO3$, which shows a well-depth of 37.2 kcal/mol. Pathways for concerted HOO-elimination were located for each β -ROO radical. However, none were submerged below the entrance channel for either ROO2 isomer or for the HOO-elimination pathway from ROO3 forming 2-ethylideneoxetane.

For each peroxy radical, the lowest energy pathway was isomerization to QOOH. Only antiradicals can form QOOH13 and QOOH23. QOOH13 and QOOH23 do not produce diastereomers because the localized electron resides on the tertiary carbon and allows the ethyl substituent to relax and become approximately planar with the ring. Only syn-peroxy radicals can form syn-QOOH14, syn-QOOH15, syn-QOOH24, and syn-QOOH25 and all retain the same stereochemistry as the respective peroxy radical precursor. For both stereoisomers of ROO1, the pathway to QOOH12 was excluded due to low (<5%) branching fraction from ROO1, which is likely due to low barriers to QOOH13 for anti-ROO1 and to syn-QOOH14 and syn-QOOH15 for syn-ROO1. For syn-QOOH15, syn-QOOH25, QOOH35, QOOH41, QOOH42, QOOH51, QOOH52, and QOOH53, the lowest energy pathway was reverse isomerization to ROO due to shallow OOOH wells.

Analogous to prototypical pathways in alkyl radical oxidation, pathways to bi-cyclic ethers were computed for each QOOH isomer, with the exception of QOOH13, syn-QOOH14, syn-QOOH24, syn-QOOH25, QOOH31, and QOOH51. These pathways

were excluded due to either large barrier heights or low branching fractions from QOOH. Low branching fractions were due to low barriers for competing pathways for ring opening and isomerization to ROO. The formation of bi-cyclic ethers was the lowest energy pathway for both QOOH21 isomers, QOOH23, QOOH32, QOOH34, and QOOH43. Notably, each are β -QOOH radicals, where the localized electron is adjacent to the –OOH group and tend to form epoxides.

Ring-opening pathways were submerged below the entrance channel for QOOH13, QOOH14, *syn*-QOOH24, and QOOH31. QOOH13 and QOOH31 both have extremely exothermic (>70 kcal/mol relative to the entrance channel) ring-opening pathways with concerted OH elimination forming 3-oxopentanal shown in **Figure 2a**. The ring-opening pathways for *syn*-QOOH14 and *syn*-QOOH24 both yield hydroperoxyalkoxy radicals as shown in **Figure 2b**. Ring-opening pathways of tertiary QOOH without concerted OH loss involved barriers that were not submerged below the entrance channel and were excluded from the rate calculations.

Figure 2. Ring-opening pathways for (a) QOOH13 and QOOH31 yield 3-oxopentanal and for (b) *syn*-QOOH14 and *syn*-QOOH24 yield hydroperoxyalkoxy radicals.

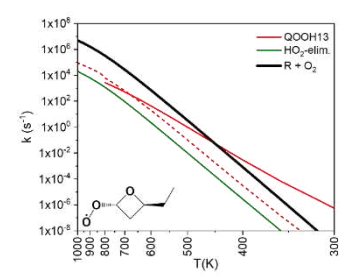
Figure 3. C–C β-scission pathways for hydroperoxy-alkoxy ring-opening. (a) syn-QOOH14, producing performic acid and 1-buten-3-yl. (b) syn-QOOH24, producing formaldehyde, trans-2-butenal, and OH.

Two consumption pathways exist for both hydroperoxyalkoxy radicals: (i) internal H-transfer and (ii) β -scission. For the first type, in both *syn*-QOOH14 and *syn*-QOOH24, the H atom from the hydroperoxyl group is transferred to the alkoxy group, yielding an unsaturated alcohol peroxy radical, which decomposes via HOO-elimination. For the second reaction type, C–C β -scission of ring-opened *syn*-QOOH14 and *syn*-QOOH24 yields performic acid + 1-buten-3-yl and formaldehyde + *trans*-2-butenal +

 $\dot{O}H$, respectively (**Figure 3**). C–O β-scission is an additional pathway for 1-hydroxypent-3-en-1-oxy in Figure 3a, which yields pent-3-enal + HOO. The C1 ketohydroperoxide, performic acid, is not reported in *n*-pentane combustion experiments, yet represents a potential chain-branching pathway. Following conventional 0-0bond-scission for ketohydroperoxide performic species, acid decomposes directly into OH + OCHO. Subsequent decomposition of OCHO yields reactive H radicals and CO_2 via a highly exothermic step [19]. In the npentane experiments of Bugler et al. [20], using a jetstirred reactor (JSR), species profiles of 2-butenal

Figure 4. β-scission pathway for QOOH35 yielding oxetan-2-one, ethene, and ÖH.

(H₃C(CH)₂CHO) were quantified as a function of temperature. Modeling predictions at 1 atm were within experimental uncertainty, yet at 10 atm were significantly overpredicted at 650 K and 825 K – the two temperatures where cyclic ether concentrations reach local maxima. The reactions in **Fig. 3** may contribute to model improvements. Only one pathway for QOOH35 is submerged below the entrance channel and is not in the aforementioned categories: a concerted β -scission reaction that yields oxetan-2-one + ethylene + \dot{O} H (**Fig. 4**).



3.2 theoretical rate coefficients

Figure 5 gives the largest rate coefficients for each stereoisomer of ROO1 at 1 atm from 300 - 1000 K. For both syn- and anti- isomers, the rate of dissociation back to R1 + O2 is higher than that of any forward reaction, which is relatively inexact due to the level of uncertainty associated with the use of phase space theory for the entrance channel rate coefficients. Since phase space theory uses the computed welldepths, yet scales the rate coefficient to match experimental rate coefficients for analogous reactions (cf. **Table 1**), the effect of the ether group on $\dot{R} + O_2$ rates introduces uncertainty. For syn-ROO1 the rate of isomerization to syn-QOOH14 and syn-QOOH15 are nearly identical from 300 - 600 K. However, two reactions that skip the syn-QOOH14 well (bi-cyclic ether formation and ring-opening) overtake the direct pathway to syn-QOOH14 and syn-QOOH15 above 600 K. HOO-elimination is not competitive with QOOH formation for either stereoisomer except for above 900 K.

Figure 6 gives the most important rate coefficients for each ROO2 stereoisomer. For each isomer, dissociation to R2 + O2, is the highest rate above 600 K. For *anti*-ROO2, the fastest reaction below 600 K is the well-skipping reaction, which forms the bi-cyclic ether, 3-ethyl-2,5-dioxabicyclo[2.1.0]pentane. For *syn*-ROO2, largest rate below 600 K is isomerization to *syn*-QOOH24.

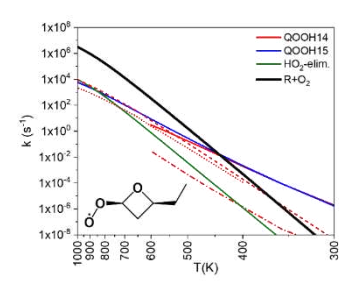
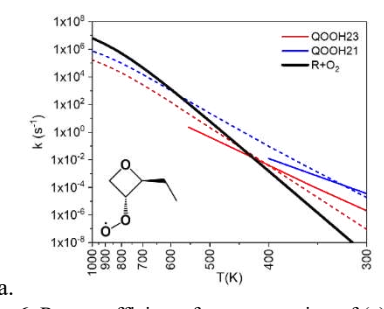


Figure 5. Rate coefficients for consumption of (a) anti-ROO1 and (b) syn-ROO1 at 1 atm from 300 - 1000 K. Solid black lines: dissociation to $\dot{R} + O_2$. Green lines: HOO-elimination. Red and blue solid lines correspond to isomerization to \dot{Q} OOH. The dotted lines correspond to well-skipping reactions where the color denotes the \dot{Q} OOH well skipped.



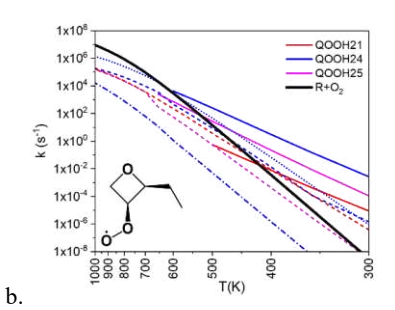


Figure 6. Rate coefficients for consumption of (a) anti-ROO2 and (b) syn-ROO2 at 1 atm from 300 - 1000 K. Solid black lines: dissociation to $\dot{R} + O_2$. Red, blue, and magenta solid lines correspond to isomerization to QOOH. The dotted lines correspond to well-skipping reactions where the color denotes the QOOH well skipped.

Figure 7 shows the highest rates for unimolecular decomposition of ROO3, ROO4, and ROO5. Above approximately 500 K, dissociation to R3 + O2 dominates. Below 500 K, isomerization to QOOH35 is favored. **Figure 7b** shows that the fastest reaction below 400 K is isomerization to QOOH42, while dissociation to R4 + O2 dominates above 400 K. **Figure 7c** shows that above 500 K, dissociation to R5 + O2 is favored, while isomerization to QOOH53 is favored below 500 K.

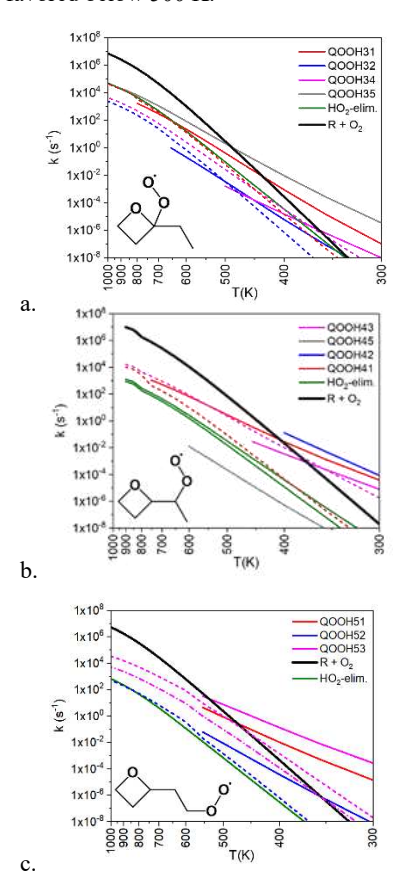


Figure 7. Rate coefficients for consumption of (a) ROO3, (b) ROO4, (c) ROO5 at 1 atm from 300 - 1000 K. The black line is dissociation to $\dot{R} + O_2$. The green line is HOÖ-elimation. The solid red, blue, magenta, and gray lines correspond to isomerization to QOOH. The dotted lines correspond to well-skipping reactions where the color denotes the QOOH well skipped.

3.3 theoretical branching fractions

Figure 8 shows the branching fractions for each 2-ethyloxetanylperoxy radical grouped by pathway type (ring-opening, HOO-elimination...) and by radical product type (OH, HOO, ...). Both of the ROO1 isomers primarily undergo ring-opening and HOO-elimination. However, *syn*-ROO1 also leads to bicyclic ether formation, and *anti*-ROO1 produces primarily OH, while *syn*-ROO1 produces primarily HOO and carbon-centered radicals. While *syn*-ROO2

primarily undergoes ring-opening, *anti*-ROO2 primarily forms bi-cyclic ethers. Both isomers yield OH predominantly.

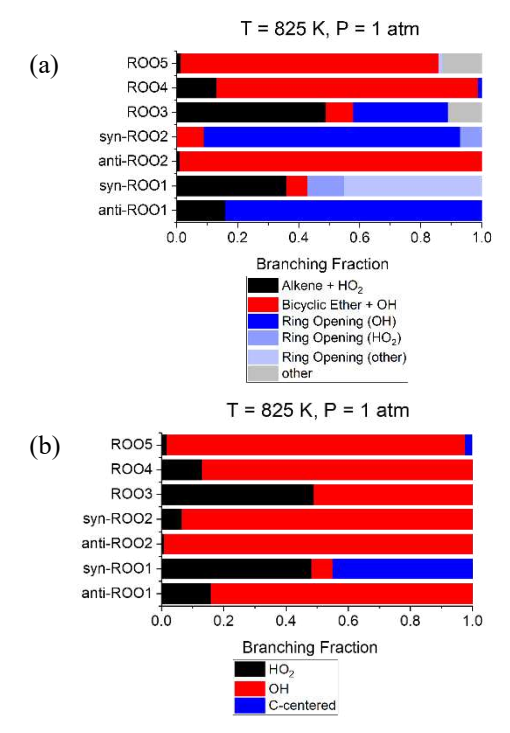


Figure 8. Branching fractions calculated from rate calculations at 20 ms, $[O_2] = 10^{12}$ molecules/cm³, 825 K, and 1 atm categorized by (a) reaction type and (b) radical product type. "other" reactions refers to β-scission reactions that are not ring-opening or HOO-elimination reactions.

Approximately 50% of ROO3 undergoes HOO-elimination. The remaining yield consists of bi-cyclic ethers, ring-opening products, and other β-scission products. ROO3 produces about half HOO and about half OH. ROO4 and ROO5 both primarily undergo bi-cyclic ether formation, yielding OH radicals. Branching fractions calculated at 650 K are similar, with some exception for reactions involving ROO1 and ROO3, and are included in S1. In general, lower-barrier pathways slightly more favored.

4. Discussion

The main purpose of the present work is to examine the reaction pathways and rates of alkyl-substituted cyclic ether oxidation on low-temperature alkane combustion, in order to inform the analysis of similar QOOH-mediated reactions in other systems. 2-ethyloxetane oxidation can impact the chemical kinetics of low-temperature combustion of *n*-pentane by altering the balance of OH and HOO radicals, the exothermicity of the decomposition of 2-ethyloxetanyl peroxy radicals, and potentially chain-branching products such as performic acid. From potential energy surface exploration with KinBot [10,

11], three classes of pathways were identified that 2ethyloxetanyl peroxy radicals follow: HOOelimination, bi-cyclic ether formation, and ringopening reactions.

The potential energy surfaces show a multitude of low-lying pathways leading to bi-cyclic ethers. Similar species were predicted in low-temperature oxidation of oxolanes from theoretical calculations vet are not conclusively identified in experiments. Several combustion studies on alkyl-substituted oxolanes [21-23] propose thermal decomposition yielding dicarbonyls as the primary consumption pathway. However, the barrier heights for such reactions likely prohibit the pathways from being significant. One plausible explanation for the lack of experimental detection, when gas chromatography is employed, is thermal decomposition of bi-cyclic ethers on the column due to combined influence of long residence times and high temperatures. In combustion reactions, decomposition of bi-cyclic ethers may more likely result from H-abstraction. Doner et al. [8] reported the potential detection of bicyclic ethers in MPIMS experiments, as indicated by ionization energy calculations as well as ion signal consistent with the molecular formula. However, unavailable reference spectra, compounded with the number of potential products with the same mass, precluded conclusive species identification.

Ring-opening with concerted OH loss produces dicarbonyls, which are also produced from ketohydroperoxide decomposition, the source of chain-branching in low-temperature combustion also observed in several cyclic ether oxidation studies [3, 4, 8, 9, 21, 22, 24]. It is critically important to characterize and account for each of these reactions so that ketohydroperoxide concentrations can be accurately determined. Additionally, because the reactions are often highly exothermic due to the release of ring-strain and the energetically favorable formation of carbonyl groups, non-Boltzmann effects [25] may arise in subsequent reactions of the resulting dicarbonyls.

Two low-lying pathways lead to performic acid (HOOC(=O)H), a ketohydroperoxide, which is 45% of the yield for *syn*-ROO1. Similar pathways were reported from two other alkyl-oxetane systems in Doner et al. [8, 9]. MPIMS experiments in Doner et al. [8] showed ion signal consistent with performic acid and peracetic acid (HOOC(=O)CH₃) in chlorine-initiated oxidation of 2-methyloxetane. However, chlorinated side-products with the same *m/z* ratio precluded definitive species identification.

Pathways via ring-opening to ketohydroperoxides are also possible for other sizes of alkyl-substituted cyclic ethers. Accordingly, whatever the effect such ketohydroperoxides impose on ignition may prove significant for combustion modeling, particularly for cases where several constitutional isomers of alkyloxetanes are formed. Such ketohydroperoxides are not present in the Bugler et al. mechanism [20, 26] for *n*-pentane oxidation. While similar species are the subject of numerous kinetics studies [27-29], none are concerned with temperatures above 400 K. Therefore,

the extent to which such species play a role in chainbranching during low-temperature combustion remains unclear. Korcek pathways are likely less favorable due to the short carbon chain, which incurs appreciable ring-strain in the first transition state of that mechanism.

Stereoisomer-dependent reaction pathways were also evident in peroxy radicals of 2,4dimethyloxetane [6], a constitutional isomer of 2ethyloxetane. By drawing comparison between the results for 2-ethyloxetanylperoxy radicals and 2,4dimethyloxetanylperoxy radicals, the effect of alkyl substituent size and position may be examined. For example, the tertiary peroxy radicals, EOROO3 and DMOROO2 (Fig. 9), are influenced significantly by interactions with alkyl substituents. For syn-DMOROO2, the peroxy group is on the opposite side of the oxetane ring plane from the distal methyl group. The orientation allows the peroxy group to abstract H from the tertiary carbon, leading to a highly favorable and exothermic ring-opening pathway, which releases OH. For anti-DMOROO2, the peroxy group and the distal methyl group are positioned on the same side of the plane of the oxetane ring, blocking access to the tertiary H-abstraction site. Therefore, the syn-DMOROO2 yields a large branching fraction towards ring-opening products compared to anti-DMOROO2, which mostly undergoes HOO-elimination. No diastereomers exist for EOROO3, and H-abstraction from C1 is not blocked by any alkyl substituent. However, the peroxy group may undergo reactions involving the ethyl substituent positioned on the same carbon. An example is the isomerization of EOROO3 to EOQOOH35 (cf. Fig. 4), which may alternatively lead to the formation of the bicyclic ether, 1,5dioxaspiro[3.3]heptane + OH. In contrast, reactions of DMOROO2 involving the methyl substituent positioned on the same carbon are limited due to the shorted chain length, increasing the ring-strain of transition states.

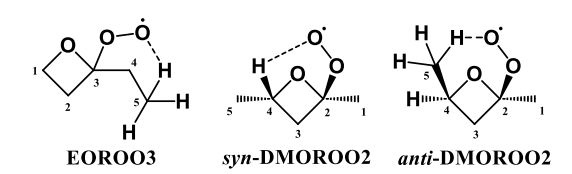


Figure 9. Comparison of ROÓ \rightarrow QOOH isomerization reactions between a peroxy radical isomer of 2-ethyloxetane from the present work and 2,4-dimethyloxetanyl peroxy radicals from Doner et al. [6], which demonstrates the impact of alkyl-substituent size and position on the reaction mechanism.

For alkyl-substituted oxetanylperoxy radicals with the peroxy group positioned on the alkyl substituent, such as EOROO4, the larger and more flexible ethyl substituent allows for more reactions involving the alkyl substituent and fewer ring-opening reactions compared to DMOROO1 (Fig. 10).

Figure 10. Comparison of ROO \rightarrow QOOH isomerization reactions between a peroxy radical isomer of 2-ethyloxetane from the present work and 2,4-dimethyloxetanyl peroxy radicals from Doner et al. [6], which illustrates the flexibility offered by a longer substituent allows for more reactions involving the alkyl substituent where the peroxy group is positioned, which compete with reactions involving the oxetane ring or other substituents and often leads to ring-opening.

From the branching fractions in the present work, the overall effect of cyclic ether oxidation on the balance of OH and HOO in the radical pool for lowtemperature alkane combustion is highly dependent on the starting distribution of peroxy radical isomers. For example, when the most abundant peroxy is radical is anti-ROO2, OH is generated across almost the entire set of pathways, which enhances ignition. However, when syn-ROO1 is the most abundant, mostly HOO and carbon-centered radicals are produced, which inhibits ignition at lower temperatures. The first step to determining the distribution of initial radicals is to obtain rate coefficients for H-abstraction by OH and HOO. The second step requires more accurate rate coefficients for the O₂-addition step. The latter is particularly important since the side to which O₂ adds determines the stereochemistry, which largely governs the radical yield. Such a task is difficult for both theoretical and experimental approaches. For such larger systems, VRC-TST [30] calculations might be somewhat more challenging to estimate the rate coefficients and branching for barrierless reactions. Furthermore, experiments are complicated by unstable intermediates and products with many constitutional isomers and stereoisomers. Branching fractions calculated herein for closed-shell intermediates produced from peroxy radical isomers that may form in oxidation experiments of 2-ethyloxetane are in S6.

Computational chemical kinetics and modeling results [5, 31, 32] demonstrate that stereochemistry impacts global observables, namely ignition delay times, and that low-temperature chain-branching of alkanes is highly sensitive to rate coefficients for cyclic ether formation [5]. The latter is due to the effect on QOOH radical populations proceeding through unimolecular reaction pathways versus second-O2-addition. Accordingly, incorporating the species and reaction pathways herein and for 2,4dimethyloxetane [6] into mechanisms for *n*-pentane combustion is expected to affect ignition and species profile predictions. However, comprehensive analysis of all cyclic ethers, and for reactions involving OOQOOH [32], is required to demonstrate in completion the effect of stereoisomers.

5. Conclusion

The present work conducted quantum chemical computations on stationary point energies along potential energy surfaces for constitutional isomers and stereoisomers of 2-ethyloxetanylperoxy in order to calculate pressure-dependent rate coefficients and produce branching fractions. Inclusion of such detailed reactions may affect ignition predictions of nalkanes because of alterations in OH and HOO populations and the existence of highly exothermic pathways. In addition, a chain-branching step leading to ketohydroperoxide-type species that, in the present case, forms from decomposition of syn-ROO1 via O-O scission and results in OH, CO2, and H. Each of these factors is controlled in part by the stereochemistry of the O2-addition step that determines the QOOH species may be formed and, in extension, which decomposition pathways are favorable. Continued expansion of sub-mechanisms for cyclic ether intermediates that includes stereochemistry is therefore critical to increasing the fidelity of combustion modeling.

Supplementary Material

S1 – potential energy surfaces

S2 – MESS input files

S3 – MESS output files

S4 - branching fraction (650 K)

S5 - differential equation script for branching fractions

 $S6-branching \ fractions \ for \ intermediates \ of \ ROO \ isomers$

Acknowledgements

BR acknowledges support by the National Science Foundation (NSF) under Grant No. 2042646. ACD was supported by NSF Grant No. 2042646 and by the U.S. Department of Energy (DOE), Office of Science, Office of Workforce Development for Teachers and Scientists, Office of Science Graduate Student Research (SCGSR) program. The SCGSR program is administered by the Oak Ridge Institute for Science and Education for the DOE under contract number DE-SC0014664. JZ is supported by the U.S. Department of Energy, Office of Science, Office of Basic Energy Sciences, Division of Chemical Sciences, Geosciences and Biosciences via the Gas Phase Chemical Physics program. JZ is an employee of National Technology & Engineering Solutions of Sandia, LLC under Contract No. DE-NA0003525 with the U.S. DOE.

References

[1] L.-S. Tran, O. Herbinet, H.-H. Carstensen, F. Battin-Leclerc, Chemical kinetics of cyclic ethers in combustion *Prog. Energy Comb. Sci.*, 92 (2022) 101019.

[2] B. Rotavera, C. A. Taatjes, Influence of functional groups on low-temperature combustion chemistry of biofuels *Progress in Energy and Combustion Science*, 86 (2021) 100025

[3] M.G. Christianson, A.C. Doner, M.M. Davis, A.L. Koritzke, J.M. Turney, H.F. Schaefer Iii, L. Sheps, D.L. Osborn, C.A. Taatjes, B. Rotavera, Reaction mechanisms of

- a cyclic ether intermediate: Ethyloxirane *International Journal of Chemical Kinetics*, 53 (2021) 43-59.
- [4] A.C. Doner, M.M. Davis, A.L. Koritzke, M.G. Christianson, J.M. Turney, H.F. Schaefer Iii, L. Sheps, D.L. Osborn, C.A. Taatjes, B. Rotavera, Isomer-dependent reaction mechanisms of cyclic ether intermediates: cis-2,3-dimethyloxirane and trans-2,3-dimethyloxirane International Journal of Chemical Kinetics, 53 (2021) 127-145
- [5] N.S. Dewey, B. Rotavera, Chemical Kinetics Analysis of Cyclic Ether Species Profiles *Combust. Flame*, 252 (2023) 112753.
- [6] A.C. Doner, J. Zádor, B. Rotavera, Stereoisomer-dependent unimolecular kinetics of 2,4-dimethyloxetanyl peroxy radicals *Faraday Discuss*, 238 (2022) 295-319.
- [7] A.C. Doner, J. Zádor, B. Rotavera, Unimolecular Reactions of 2,4-Dimethyloxetanyl Radicals *J. Phys. Chem. A*, 127 (2023) 2591-2600.
- [8] A.C. Doner, N.S. Dewey, B. Rotavera, Unimolecular Reactions of 2-Methyloxetanyl and 2-Methyloxetanylperoxy Radicals *J. Phys. Chem. A*, 127 (2023) 6816-6829.
- [9] A.C. Doner, J. Zádor, B. Rotavera, Stereoisomer-dependent unimolecular kinetics of 2,4-dimethyloxetanyl peroxy radicals *Faraday Discussions*, 238 (2022) 295-319.
- [10] R. Van de Vijver, J. Zádor, KinBot: Automated stationary point search on potential energy surfaces *Computer Physics Communications*, 248 (2020) 106947.
- [11] J. Zádor, C. Martí, R. Van de Vijver, S.L. Johansen, Y. Yang, H.A. Michelsen, H.N. Najm, Automated Reaction Kinetics of Gas-Phase Organic Species over Multiwell Potential Energy Surfaces *The Journal of Physical Chemistry A*, 0 (2023) null.
- [12] Gaussian16 Revision C .01, 2016.
- [13] F. Neese, Software update: the ORCA program system, version 4.0 WIREs Computational Molecular Science, 8 (2018) e1327.
- [14] MESS.2016.3.23 Computer Program,
- [15] P. Pechukas, J.C. Light, On Detailed Balancing and Statistical Theories of Chemical Kinetics *The Journal of Chemical Physics*, 42 (2004) 3281-3291.
- [16] D. Wu, K.D. Bayes, Rate constants for the reactions of isobutyl, neopentyl, cyclopentyl, and cyclohexyl radicals with molecular oxygen *International Journal of Chemical Kinetics*, 18 (1986) 547-554.
- [17] T.M. Lenhardt, C.E. McDade, K.D. Bayes, Rates of Reaction of Butyl Radicals with Molecular-Oxygen *Journal of Chemical Physics*, 72 (1980) 304-310.
- [18] A.W. Jasper, "Third-body" collision parameters for hydrocarbons, alcohols, and hydroperoxides and an effective internal rotor approach for estimating them *Int. J. Chem. Kin.*, 52 (2020) 387-402.
- [19] P. Marshall, P. Glarborg, Ab initio and kinetic modeling studies of formic acid oxidation *Proceedings of the Combustion Institute*, 35 (2015) 153-160.
- [20] B. John, R. Anne, H. Olivier, B.-L. Frédérique, T. Casimir, D. Guillaume, D. Philippe, J.C. Henry, An experimental and modelling study of n-pentane oxidation in two jet-stirred reactors: The importance of pressure-dependent kinetics and new reaction pathways *Proceedings of the Combustion Institute*, 36 (2017) 441-448.
- [21] G. Vanhove, Y. Yu, M.A. Boumehdi, O. Frottier, O. Herbinet, P.-A. Glaude, F. Battin-Leclerc, Experimental Study of Tetrahydrofuran Oxidation and Ignition in Low-Temperature Conditions *Energy & Fuels*, 29 (2015) 6118-6125.

- [22] F. Yann, G. Adrià, V. Guillaume, C. Hans-Heinrich, M. Kevin, R.W. Phillip, H. Olivier, B.-L. Frédérique, A model of tetrahydrofuran low-temperature oxidation based on theoretically calculated rate constants *Combustion and Flame*, 191 (2018) 252-269.
- [23] Y. Fenard, M.A. Boumehdi, G. Vanhove, Experimental and kinetic modeling study of 2-methyltetrahydrofuran oxidation under engine-relevant conditions *Combustion and Flame*, 178 (2017) 168-181.
- [24] J.C. Davis, A.L. Koritzke, R.L. Caravan, I.O. Antonov, M.G. Christianson, A.C. Doner, D.L. Osborn, L. Sheps, C.A. Taatjes, B. Rotavera, Influence of the Ether Functional Group on Ketohydroperoxide Formation in Cyclic Hydrocarbons: Tetrahydropyran and Cyclohexane *The Journal of Physical Chemistry A*, 123 (2019) 3634-3646.
- [25] C.R. Mulvihill, A.D. Danilack, C.F. Goldsmith, M. Demireva, L. Sheps, Y. Georgievskii, S.N. Elliott, S.J. Klippenstein, Non-Boltzmann Effects in Chain Branching and Pathway Branching for Diethyl Ether Oxidation *Energy & Fuels*, 35 (2021) 17890-17908.
- [26] B. John, P. Jennifer, J.C. Henry, A theoretical study of cyclic ether formation reactions *Proceedings of the Combustion Institute*, 36 (2017) 161-167.
- [27] Z. Yuan, Y. Ni, A.R.P. Van Heiningen, Kinetics of peracetic acid decomposition: Part I: Spontaneous decomposition at typical pulp bleaching conditions *The Canadian Journal of Chemical Engineering*, 75 (1997) 37-41.
- [28] T. Zhang, C.-H. Huang, Modeling the Kinetics of UV/Peracetic Acid Advanced Oxidation Process Environmental Science & Technology, 54 (2020) 7579-7590. [29] E. Santacesaria, V. Russo, R. Tesser, R. Turco, M. Di Serio, Kinetics of Performic Acid Synthesis and Decomposition Industrial & Engineering Chemistry Research, 56 (2017) 12940-12952.
- [30] Y. Georgievskii, S.J. Klippenstein, Variable reaction coordinate transition state theory: Analytic results and application to the $C_2H_3+H\rightarrow C_2H_4$ reaction *The Journal of Chemical Physics*, 118 (2003) 5442-5455.
- [31] S. Y. Mohamed, A. C. Davis, M. J. Al Rashidi, S. M. Sarathy, High-Pressure Limit Rate Rules for α -H Isomerization of Hydroperoxyalkylperoxy Radicals *J. Phys. Chem. A* 122 (2018) 3626–3639.
- [32] A. D. Danilack, C. R. Mulvihill, S. J. Klippenstein, C. F. Goldsmith, Diastereomers and Low-Temperature Oxidation, *J. Phys. Chem. A* 125 (2021) 8064–8073.